

# Application of a Coupled High-Order FEM Solver to Aeroengine Exhaust Noise

Karim Hamiche  
Siemens Industry Software NV, Belgium.

Gwénaél Gabard  
Laboratoire d'Acoustique de l'Université du Mans, France.

Hadrien Bériot  
Siemens Industry Software NV, Belgium.

Sophie Le Bras  
Siemens Industry Software NV, Belgium.

## Abstract

In this study, the Linearised Euler Equations are coupled to the Linearised Potential Equation in order to simulate sound propagation in complex non-uniform mean flows at a reasonable computational cost. The coupling technique is formulated in the frequency domain in a high-order finite element framework. It consists in enforcing physical continuity conditions between the scalar velocity potential and the linearised Euler state vector at the coupling interface. The performance of the coupling is evaluated by simulating the sound radiation from an aeroengine exhaust with a strongly non-uniform mean flow. The numerical results are successfully compared with a reference solution, demonstrating that the coupling enables a proper representation of the acoustic and vorticity waves, as well as the refraction of the sound field across the jet shear layer. Significant benefits in terms of memory requirements and computational time are also obtained in comparison with the full linearised Euler solution.

PACS no. 43.28.Js, 43.28.Py

## 1. Introduction

Sound propagation in complex non-uniform mean flows is an important research area for transport, building and power generation industries. In particular, the prediction of sound radiated from turbofan engines is critical in the aerospace industry in order to meet environmental regulations [1]. In rotating and pulsating machines, the sound waves generated from unsteady flows propagate in ducts and eventually radiate through their openings. The presence of duct discontinuities and complex mean flow effects strongly influences the acoustic propagation [2].

The acoustic propagation in the presence of a mean flow can be solved using several models, amongst which the convected Helmholtz equation for uniform flows [3] or the Linearised Potential Equation (LPE) for irrotational flows [4]. These equations present the advantage of solving a single unknown, yielding relatively low computational costs. However, they ac-

count neither for the complexity of multidirectional sheared flows and the refraction through shear layers, nor for the vorticity/entropy waves and their interactions [5]. These physical effects, of crucial importance for acoustic propagation, are supported by the Linearised Euler Equations (LEE). But this more general physical model is much more costly to solve numerically, since it involves up to five unknowns.

Solving the LEE in the time domain presents two major drawbacks, namely the existence of physical linear Kelvin-Helmholtz instabilities due to the absence of non-linear and viscous effects normally present in real flows [6], and the complexity in modelling impedance boundary conditions [7]. An alternative approach is to solve the LEE in the frequency domain using the Finite Element Method (FEM). Furthermore, the computational cost can be reduced by solving the LEE using a high-order FEM approach [8]. This method, referred to as  $p$ -FEM in the following, benefits from the use of high-order shape functions. In addition, the FEM is known to suffer from numerical instabilities in convection-dominated problems due to a lack of diffusion in the formulation [9]. This

can be corrected by adding artificial diffusion terms such as in the Galerkin/Least-Squares (GLS) formulation [10, 11]. Another important modelling aspect is the choice of non-reflecting boundary conditions for exterior noise propagation. The Perfectly Matched Layer (PML) technique introduced by Bérenger [12] for the absorption of electromagnetic waves is well suited for this kind of problems: the wave amplitude is gradually decreased in an additional layer through an adequate change of coordinates into the complex space, allowing to limit the spurious reflections into the computational domain.

In this paper, an innovative approach is presented in order to simulate the acoustic radiation from aero-engine exhausts at a reasonable computational cost. The main idea is to solve the LEE in the regions of strong mean flow gradients, while applying the LPE in the regions where the mean flow can be approximated as potential. For this purpose, coupling conditions are defined at the interface between the LEE and the LPE subdomains: the physical continuity of the solution at the interface is ensured by expressing the set of variables on each side of the interface in terms of the other set of variables. In this study, a stabilised axisymmetric form of the LEE is combined with an axisymmetric LPE formulation. The coupling methodology is first validated by simulating the acoustic propagation in a duct and by computing the numerical error with respect to a reference analytical solution. The method is then applied to an aero-engine exhaust test case with non-uniform mean flow: an acoustic wave propagates through the exhaust nozzle and radiates outside. A good agreement between the LEE/LPE coupling solution and the full LEE reference solution is obtained. The benefits in terms of computational costs are also demonstrated. The paper is organised as follows. The model equations are first presented in Section 2. Next, the high-order finite element framework and the LEE/LPE coupling are described in Section 3. The numerical results including the validation of the coupling strategy are then shown in Section 4. Finally, conclusions are drawn in Section 5.

## 2. Physical Model

### 2.1. Linearised Euler Equations

The Navier-Stokes equations are written for a perfect gas with isentropic disturbances, no viscous effect, no heat transfer and no external source. The Linearised Euler Equations are then obtained for the time-harmonic perturbation vector  $\mathbf{q}'$ , where the superscript  $'$  indicates the small perturbations around a steady mean flow. This variable vector includes the fluctuations of the mass density  $\rho$ , the momentum vector  $\rho\mathbf{u}$  ( $\mathbf{u}$  being the velocity vector) and the non-dimensional pressure defined by Goldstein

$p_c = (p/p_\infty)^{(1/\gamma)}$  (with  $p$  the pressure,  $p_\infty$  a reference pressure and  $\gamma$  the specific heat ratio) [13].

In this study, the cylindrical coordinates  $(r, \theta, x)$  are used. This coordinate system is convenient since mean flows and geometries are often axisymmetric, leading to a Fourier decomposition of the solution vector of the following type:

$$\mathbf{q}'(r, \theta, x, t) = \mathbf{q}'(r, x)e^{-jm\theta}e^{j\omega t}, \quad (1)$$

where  $\mathbf{q}' = [\rho'; (\rho u_r)'; (\rho u_\theta)'; (\rho u_x)'; p'_c]$ ,  $m \in \mathbb{Z}$  is the azimuthal order,  $\omega$  is the angular frequency and  $t$  is the time. The LEE thus write as:

$$\begin{aligned} \mathcal{L}(\mathbf{q}') &= \left( j\omega - j\frac{m}{r}\mathbf{A}_\theta + \frac{1}{r}\mathbf{A}_c \right) \mathbf{q}' \\ &+ \frac{1}{r} \frac{\partial}{\partial r} r \mathbf{A}_r \mathbf{q}' + \frac{\partial \mathbf{A}_x \mathbf{q}'}{\partial x} = 0, \end{aligned} \quad (2)$$

where  $\mathcal{L}(\mathbf{q}')$  is the differential operator for the LEE, and  $\mathbf{A}_r$ ,  $\mathbf{A}_\theta$ ,  $\mathbf{A}_x$  and  $\mathbf{A}_c$  are square matrices dependent on the mean flow variables, namely: the mass density  $\rho_0$ , the speed of sound  $c_0$ , the velocity vector  $\mathbf{u}_0$ , and the pressure  $p_0$  [14].

### 2.2. Linearised Potential Equation

In the full potential theory, the velocity field  $\mathbf{u}$  is irrotational and can be written as the gradient of a velocity potential  $\phi$  of a fluid element traveling along a streamline. The mean and fluctuating velocity components thus read:  $\mathbf{u}_0 = \nabla\phi_0$  and  $\mathbf{u}' = \nabla\phi'$ . The LPE follows:

$$\rho_0 \frac{d_0}{dt} \left( \frac{1}{c_0^2} \frac{d_0\phi'}{dt} \right) - \nabla \cdot (\rho_0 \nabla\phi') = 0, \quad (3)$$

where  $d_0/dt = j\omega + \mathbf{u}_0 \cdot \nabla$  is the material derivative.

### 2.3. Duct Modes

Duct modes form a complete basis for the duct incident wave and are used to describe acoustic sources [15]. For cylindrical ducts with uniform axial mean flow velocity  $u_0 = u_{0,x}$ , each duct mode can be written as:

$$p'_{c_{m,n}}(r, \theta, x) = a_{m,n} U_{m,n}(r) e^{-jk_{x_{m,n}}x} e^{-jm\theta}, \quad (4)$$

where  $n \in \mathbb{N}^*$  is the radial order,  $a_{m,n}$  is the amplitude,  $U_{m,n}$  is the radial shape function, and  $k_{x_{m,n}}$  is the axial wavenumber. The radial shape function for circular ducts depends on the  $m^{\text{th}}$ -order Bessel function of the first kind and on the radial wavenumber  $k_{r_{m,n}} = \alpha_{m,n}/r_d$ , where  $\alpha_{m,n}$  is the  $n^{\text{th}}$ -zero of the characteristic equation and  $r_d$  is the duct outer radius [5, 15].

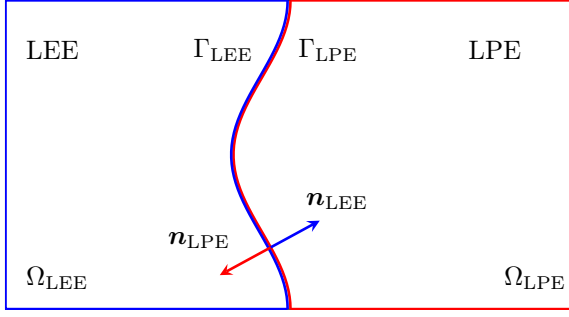


Figure 1: Coupling configuration between two subdomains.

### 3. High-Order Finite Element Model

The computational domain  $\Omega$  is decomposed into two subdomains,  $\Omega_{LEE}$  for the LEE subdomain and  $\Omega_{LPE}$  for the LPE subdomain such that  $\Omega = \Omega_{LEE} \cup \Omega_{LPE}$ . The subdomain boundaries are noted  $\Gamma_{LEE}$  and  $\Gamma_{LPE}$ , with the unit normal vectors  $\mathbf{n}_{LEE}$  and  $\mathbf{n}_{LPE}$  pointing towards the exterior of their respective domains. Figure 1 shows the configuration of the computational domain with LEE/LPE coupling interface.

#### 3.1. LEE Formulation

The weak form of the weighted residual formulation derived from Equation (2) for the LEE yields:

$$\begin{aligned} & \int_{\Omega_{LEE}} \left( j\omega r \mathbf{w}^T \mathbf{q}' - jm \mathbf{w}^T \mathbf{A}_\theta \mathbf{q}' + \mathbf{w}^T \mathbf{A}_c \mathbf{q}' \right. \\ & \quad \left. - r \frac{\partial \mathbf{w}^T}{\partial r} \mathbf{A}_r \mathbf{q}' - r \frac{\partial \mathbf{w}^T}{\partial r} \mathbf{A}_x \mathbf{q}' \right) dr dx \\ & + \sum_i \int_{\Omega_{LEE_i}} \mathcal{D}(\mathbf{w})^T \tau_i \mathcal{L}(\mathbf{q}') d\Omega_{LEE_i} \\ & = - \int_{\Gamma_{LEE}} r \mathbf{w}^T \mathbf{F} \mathbf{q}' d\Gamma, \end{aligned} \quad (5)$$

where  $\mathbf{w}$  is the weighting function vector, and  $\mathbf{F} = n_x \mathbf{A}_x + n_r \mathbf{A}_r$  is the flux matrix,  $n_x$  and  $n_r$  being the components of the outgoing unit normal vector to the boundary  $\Gamma_{LEE}$ . The superscript  $T$  denotes the Hermitian transpose. The stabilisation term  $\mathcal{D}(\mathbf{w})^T \tau_i$  in the left-hand side of Equation (5) is defined within each element as the product of the stabilisation operator  $\mathcal{D}(\mathbf{w})$  and the stabilisation parameter  $\tau_i$ . In this study, the GLS stabilisation operator is used [10]:

$$\begin{aligned} \mathcal{D}(\mathbf{w}) &= \left( j\omega - j \frac{m}{r} \mathbf{A}_\theta^T + \frac{1}{r} \mathbf{A}_c^T \right) \mathbf{w} \\ & \quad + \frac{1}{r} \frac{\partial r \mathbf{A}_r^T \mathbf{w}}{r} + \frac{\partial \mathbf{A}_x^T \mathbf{w}}{\partial x}. \end{aligned} \quad (6)$$

Following Rao and Morris [11], the stabilisation parameter is defined as  $\tau_i = \max(\alpha h_{i,l} / \lambda_l) \mathbf{I}$ , where  $\alpha$  is a stabilisation coefficient,  $h_{i,l}$  is the element size in the  $l^{\text{th}}$ -direction,  $\lambda_l$  is the spectral radius of the coefficient

matrix  $\mathbf{A}_l$ , and  $\mathbf{I}$  is the identity matrix. In the simulations, the coefficient  $\alpha$  is set to  $\alpha = 1/(2p)$ . The factor  $1/p$  accounts for the high-order shape functions, and the factor  $1/2$  gives a value of  $\tau_i$  analogous to the steady convective-diffusive equation [9].

#### 3.2. LPE Formulation

Introducing the test function  $w$  for the axisymmetric LPE and considering the velocity component  $u_{0\theta} = 0$ , the weighted residual formulation for the LPE reads:

$$\begin{aligned} & \int_{\Omega_{LPE}} \left( -r \frac{\rho_0}{c_0^2} \frac{d_0 \bar{w}}{dt} \frac{d_0 \phi'}{dt} + r \rho_0 \nabla \bar{w} \cdot \nabla \phi' + \frac{m^2}{r} \rho_0 \bar{w} \phi' \right) dr dx \\ & = - \int_{\Gamma_{LPE}} \frac{\rho_0}{c_0^2} r \bar{w} \left( (u_{0n}^2 - c_0^2) \frac{\partial \phi'}{\partial n} + u_{0n} u_{0\tau} \frac{\partial \phi'}{\partial \tau} \right) d\Gamma \\ & \quad - \int_{\Gamma_{LPE}} j \frac{\rho_0}{c_0^2} r \omega u_{0n} \bar{w} \phi' d\Gamma, \end{aligned} \quad (7)$$

where  $u_{0n}$  is the normal mean flow velocity,  $u_{0\tau}$  the tangential mean flow velocity, and the overline  $\bar{\cdot}$  denotes the complex conjugate.

#### 3.3. Coupling Methodology

At the interface between the two subdomains  $\Omega_{LEE}$  and  $\Omega_{LPE}$ , appropriate coupling conditions are required in order to ensure the acoustic propagation through the interface. To this end, the boundary integrals in the formulations (5) and (7) are expressed as functions of the variables of the other subdomain.

For the LPE side, the generalised Robin boundary condition is used in order to represent the transmission of the acoustic characteristics propagating along the normal vector to the boundaries:

$$\frac{\partial \phi'}{\partial n} + j k_c^+ \phi' = g_n, \quad (8)$$

where  $g_n$  is the source term denoting the acoustic characteristic traveling along the normal vector  $\mathbf{n}$ , and  $k_c^+ = \omega / (c_0 + u_{0n})$  is the outgoing acoustic wavenumber. The quantity  $g_n$  is prescribed from the LEE as:

$$g_{n_{LPE}} = \frac{\partial \phi'}{\partial n_{LPE}} + j k_c^+ \phi', \quad (9)$$

where the velocity potential is computed from the LEE variables as:

$$\phi' = \frac{1}{j\omega\rho_0} \left( (u_0^2 - c_0^2) \rho' - \mathbf{u}_0 \cdot (\rho \mathbf{u}') \right). \quad (10)$$

The expression of  $\partial \phi' / \partial n$  in Equation (8) is then replaced in Equation (7), leading to a boundary integral with contribution terms from the incoming waves:

$$B_{LPE} = - \int_{\Gamma_{LPE}} \frac{\rho_0}{c_0^2} r (u_{0n_{LPE}}^2 - c_0^2) \bar{w} g_{n_{LEE}} d\Gamma, \quad (11)$$

where  $u_{0n_{LPE}} = \mathbf{u}_0 \cdot \mathbf{n}_{LPE}$ .

For the LEE side, the flux  $\mathbf{F}$  in the boundary integral of Equation (5) is decomposed into the contributions of two flux matrices  $\mathbf{F}^+$  and  $\mathbf{F}^-$ , containing the outgoing and incoming characteristics, respectively. In the coupling strategy, only the incoming characteristics are imposed, yielding the following coupling integral:

$$B_{\text{LEE}} = - \int_{\Gamma_{\text{LEE}}} r \mathbf{w}^T \mathbf{F}^- \mathbf{q}'_{\text{LPE}} d\Gamma, \quad (12)$$

where the variable vector  $\mathbf{q}'_{\text{LPE}}$  is built from the velocity potential  $\phi'$  computed in the LPE domain:

$$\mathbf{q}'_{\text{LPE}} = \rho_0 \begin{pmatrix} 0 \\ \frac{\partial}{\partial r} \\ -j \frac{m}{r} \\ \frac{\partial}{\partial x} \\ 0 \end{pmatrix} \phi' - \frac{\rho_0}{c_0^2} \begin{pmatrix} 1 \\ u_{0r} \\ u_{0\theta} \\ u_{0x} \\ \frac{p_{c0}}{\rho_0} \end{pmatrix} \frac{d_0 \phi'}{dt}. \quad (13)$$

This coupling method combines two sets of equations which do not support the same waves: while the LPE only supports the right- and left-propagating acoustic waves, the LEE also account for the vorticity and the entropy waves. Thus, in order to avoid spurious reflections, the boundary interface between the LEE and LPE subdomains must be located in a region where the amplitude of the vorticity and entropy waves is negligible. In the framework of aeroengine noise, as the vorticity waves develop along the jet shear layer as a vortex shedding, the boundary interface should therefore not be defined in that region.

### 3.4. Finite Element Model

From the integral formulations (5) and (7), a linear system  $\mathbf{K}\mathbf{s} = \mathbf{f}$  is obtained, where the complex-valued sparse matrix  $\mathbf{K}$  contains the different contributions of the physical integrals from both subdomains, and their coupling terms  $B_{\text{LEE}}$  and  $B_{\text{LPE}}$ . The vectors  $\mathbf{s}$  and  $\mathbf{f}$  are the solution and source vectors, respectively. The matrix  $\mathbf{K}$  can be written as:

$$\mathbf{K} = \begin{bmatrix} \mathbf{K}_{11} & \mathbf{C}_{12} \\ \mathbf{C}_{21} & \mathbf{K}_{22} \end{bmatrix}, \quad (14)$$

where  $\mathbf{K}_{11}$  and  $\mathbf{K}_{22}$  are the system matrices relative to the LEE and LPE subdomains respectively, and  $\mathbf{C}_{12}$  and  $\mathbf{C}_{21}$  are the coupling matrices between the two subdomains.

In the  $p$ -FEM solver, the standard linear basis is enriched with edge and bubble shape functions. The Lobatto shape functions are used in the numerical simulations for their hierarchic property and their good conditioning [8]. In the simulations, specific boundary conditions are applied at the walls and at the external boundaries of the domain. More precisely, an axial symmetry condition is enforced along the boundary at  $r = 0$  and hard-wall conditions ( $u_{0n} = u'_n = 0$ , where  $u'_n$  is the normal velocity perturbation) are specified at the engine duct walls.

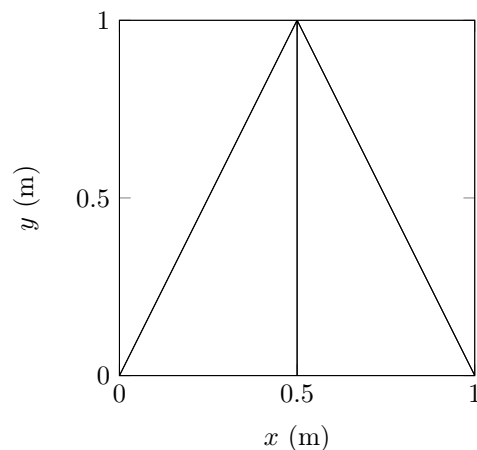


Figure 2: Computational domain and mesh for the duct test case (coupling interface at  $x = 0.5$  m).

PML are applied to inject the modes inside the duct and to absorb the outgoing waves in the far-field region. More details on the application of the boundary conditions can be found in [5, 16].

The calculations presented in this paper have been performed in a Matlab computing environment using a standard computer (Intel Core i7 2.7 GHz, 32 Go RAM) [17].

## 4. Numerical Results

In this section, the validity of the LEE/LPE coupling methodology is verified by simulating a duct propagation test case. The coupling method is then applied to compute the sound radiated from a simplified aeroengine exhaust.

### 4.1. Duct Test Case

Let us consider an infinite duct where an acoustic plane wave propagates in the  $x$ -direction, in the presence of a uniform mean flow defined by a Mach number  $M_0 = u_0/c_0 = 0.6$ , a density  $\rho_0 = 1.225 \text{ kg/m}^3$  and a speed of sound  $c_0 = 340.27 \text{ m/s}$ . A two-dimensional  $(x, y)$ -section of the duct is modeled using a square computational domain, such that both  $x$  and  $y$  range from 0 to 1 m, as shown in Figure 2. Characteristic boundary conditions are applied at the external boundaries of the domain in order to ensure the acoustic propagation. An unstructured mesh composed of triangular elements is used with a characteristic mesh size  $h = 0.5 \text{ m}$ .

Two test cases are considered. In the first case, the whole domain is solved using the LEE. In the second case, the computational domain is divided into a LEE and a LPE regions separated by a plane interface located at  $x = 0.5 \text{ m}$  (see Figure 2). In order to evaluate the performance of the LEE/LPE coupling in terms

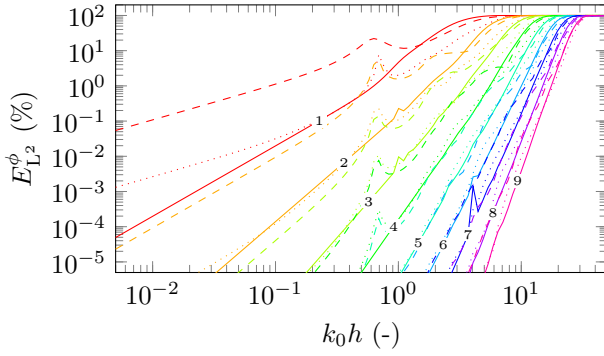


Figure 3: Error  $E_{L^2}^{\phi}$  against the Helmholtz number, for an acoustic plane wave in a two-dimensional duct. Solid line: no coupling, full LEE. Dashed line: LEE/LPE coupling, with  $p_{\text{int}} = p$ . Dotted line: LEE/LPE coupling, with  $p_{\text{int}} = p + 1$ .

of accuracy, the  $L^2$ -norm error  $E_{L^2}$  between the numerical solution and the analytical solution is computed for the velocity potential. Figure 3 presents the error levels obtained from the full LEE computation (solid line) and from the LEE/LPE coupling computation (dashed line) against the characteristic Helmholtz number  $k_0 h$ , where the wavenumber  $k_0$  varies from  $0.01 \text{ m}^{-1}$  to  $100 \text{ m}^{-1}$ , and the polynomial order  $p$  from 1 to 9. It is observed that the  $L^2$ -norm convergence in the high-resolution regime is of order  $p$  for the LEE/LPE coupling solution, whereas it is of order  $p + 1$  for the full LEE solution. This is due to the presence of the gradient components  $\partial\phi'/\partial n$  and  $\partial\phi'/\partial\tau$  in the coupling strategy (see Equations (9) and (13)). These terms are obtained from the differentiation of the velocity potential  $\phi'$  along the interface, which deteriorates by one order the accuracy of the scheme. In order to circumvent this loss of accuracy, the polynomial order  $p_{\text{int}}$  in the elements along the coupling interface can be incremented by 1. The error levels thus obtained are displayed in dotted line in Figure 3. In this case, the convergence rates are similar to those obtained without coupling. These results demonstrate the validity of the proposed coupling method in the framework of a high-order finite element scheme. More details on this validation case can be found in [5].

#### 4.2. Aeroengine Exhaust Acoustic Propagation

The LEE/LPE coupling strategy is applied to simulate the sound radiated from a straight circular semi-infinite duct [18]. The duct is characterised by a radius  $r_d = 1 \text{ m}$  and infinitely thin walls. Its geometry is displayed in Figure 4. The mean flow velocity is oriented in the axial direction  $x$ , and defined by a Mach number  $M_d = 0.5$  in the duct and  $M_o = 0$  in the outer region. Turbofan exhaust mean flows are characterised by shear layers with strong velocity gradients. In order to reproduce these conditions, the mean flow

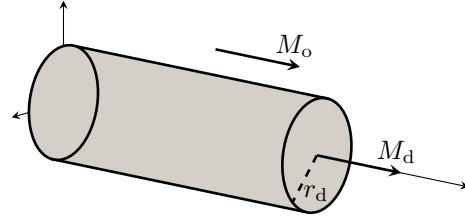


Figure 4: Straight circular duct geometry of the aeroengine exhaust.

Mach number in the shear layer is imposed from the following analytical profile:

$$M(r, x) = \bar{M} \left( 1 + \tanh \left( \frac{r_d - |r|}{\zeta \delta(x)} \right) \right), \quad (15)$$

where  $\bar{M} = (M_d + M_o)/2$  is the mean value of the Mach number,  $\zeta = 2/5 \cos^2(\beta/2)$  is a parameter to control the shear layer profile,  $\beta = 20^\circ$  is the spreading angle and  $\delta$  is the shear layer thickness given by:

$$\delta(x) = 2(x - x_d) \tan(\beta/2). \quad (16)$$

In the ambient medium, the mean flow density, the speed of sound and the specific heat ratio are uniform and respectively have the following values:  $\rho_0 = 1.225 \text{ kg/m}^3$ ,  $c_0 = 340.27 \text{ m/s}$  and  $\gamma = 1.4$ . At the duct inlet, an acoustic duct mode  $(m, n) = (10, 1)$  is injected inside the pipe with the angular frequency  $\omega = 5785 \text{ rad/s}$  and the Helmholtz number  $k_0 r_d = 17$ .

In order to capture the non-uniform mean flow effects, the shear layer region is solved using the LEE. In the rest of the domain where the mean flow is irrotational, the LPE is applied. The computational domain considered in this study is presented in Figure 5. It extends from  $x = 0$  to  $5 \text{ m}$  axially and from  $r = 0$  to  $2.5 \text{ m}$  radially. The duct exit plane is located at  $x_d = 2.5 \text{ m}$ . The coupling interface between the LEE and the LPE regions is shown in Figure 6, where the mean flow Mach number contours are displayed, as well as in Figure 5. It surrounds the duct trailing edge and is deliberately located at a distance of  $0.2 \text{ m}$  from the geometrical singularity in order to avoid the production of spurious reflections due to the vortex sheet generated there.

At the duct inlet and on the external boundaries of the domain, PML are applied. The PML are one-element wide, with a length of  $0.2 \text{ m}$ . On the duct walls, hard-wall boundary conditions are imposed. Axisymmetric boundary conditions are applied at  $r = 0$  along the axis  $x$ . Finally, the coupling conditions introduced in Section 3.3 are implemented along the coupling interface between the LEE and the LPE regions.

The spatial discretisation is carried out using an unstructured mesh mainly composed of triangular elements, as shown in Figure 5. More precisely, in the

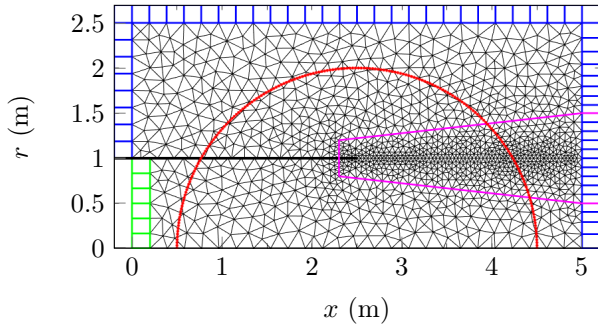


Figure 5: Computational domain, mesh, points where the SPL is computed (red dots), and coupling interface (magenta dotted lines).

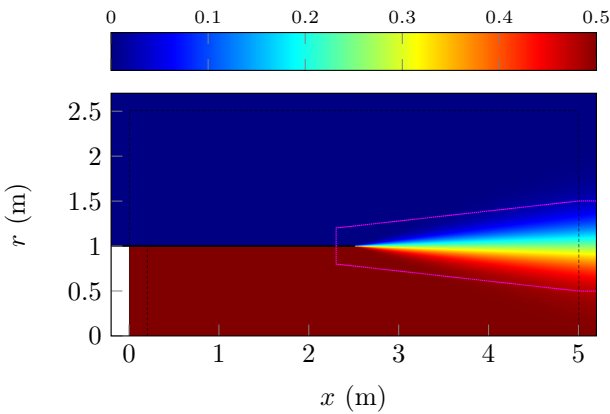


Figure 6: Mean flow Mach number contours.

shear layer, the grid spacing in the axial direction is equal to 0.04 m in order to capture the vorticity shedding developing from the duct trailing edge. In the rest of the domain, a mesh size of about 0.2 m is imposed. These element characteristic dimensions are chosen with respect to the shortest acoustic and vorticity wavelengths, which in this example are both equal to 0.18 m. The use of high-order shape functions prevents from having to use too small elements. The computational domain then contains 1272 elements in the LEE subdomain and 1367 elements in the LPE subdomain yielding the following ratio  $\tau_{\text{LEE/LPE}}^e = 48.2\%$ . This means that 48.2% of the elements are concentrated in the LEE domain while 51.8% of the elements lie in the LPE domain.

In order to evaluate the benefits of using the LEE/LPE coupling strategy in terms of memory requirements and computational time, another simulation has been carried out applying the LEE in all the computational domain. The two computations are performed using a polynomial order  $p = 8$ .

The contours of the real part of the non-dimensional pressure and  $x$ -momentum obtained in the simulation performed with the LEE/LPE coupling are shown in Figures 7 and 8, respectively. The solution is continu-

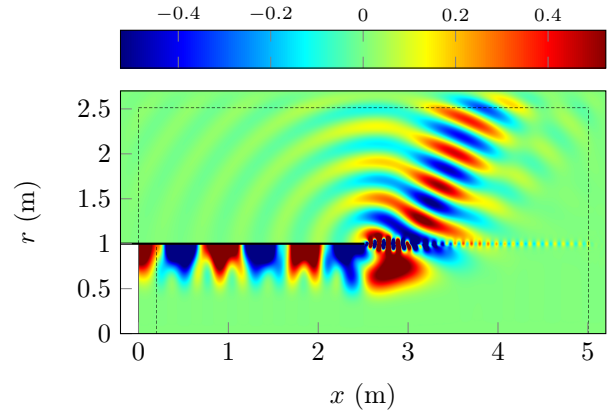


Figure 7: Real part of the non-dimensional pressure, obtained with the LEE/LPE coupling simulation.

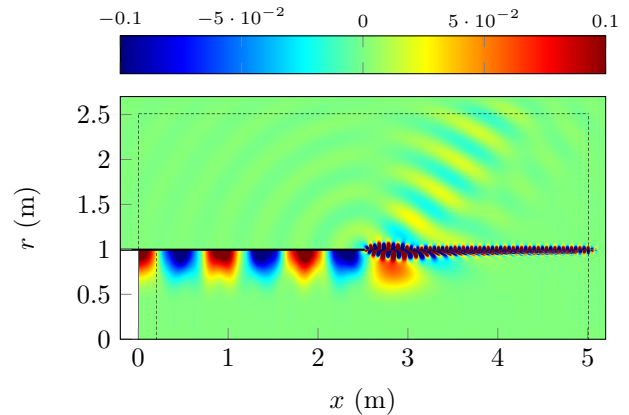


Figure 8: Real part of the  $x$ -momentum ( $\text{kg/m}^2/\text{s}$ ), obtained with the LEE/LPE coupling simulation.

ous across the coupling interface. Sound propagation, refraction and radiation effects are also visible. In addition, the shear layer is responsible for the generation of the hydrodynamic Kelvin-Helmholtz instability, which develops as a vorticity shedding along the duct wake and decays after a finite distance.

The Sound Pressure Level (SPL) is computed at points located on a circle of radius 2 m centred at  $(x = 2.5 \text{ m}, r = 0)$ . This circle is shown in red in Figure 5. The corresponding directivities obtained from the simulation with the LEE/LPE coupling and from the full LEE computation are shown in Figure 9. The direction given by the angle  $\Phi = 0^\circ$  is aligned with the positive  $x$ -direction. The results are compared to an analytic solution obtained without vorticity shedding and used as a reference solution [19]. A good agreement is observed between the analytical and numerical solutions. In particular, the vortex sheet does not significantly impact the acoustic directivity outside of the duct wake. Close to  $\Phi = 30^\circ$ , a peak corresponding to the vortex sheet is observed. This peak is not visible on the reference solution, since the Kutta con-

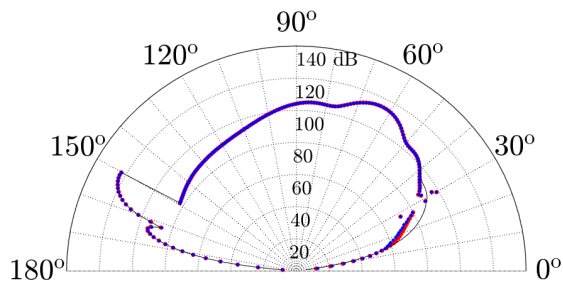


Figure 9: SPL directivity for points located on a circle of radius 2 m and of centre ( $x = 2.5$  m,  $r = 0$ ). Black solid line: analytical solution. Red dots: full LEE solution. Blue dots: LEE/LPE coupling solution.

dition is not applied. The non-uniform mean flow is responsible for the wave refraction outside the duct. The SPL plot also shows that the coupled model solution nicely matches the full LEE solution, in both the LEE and the LPE subdomains. Some discrepancies are observed near the symmetry axis for  $\Phi < 20^\circ$  where the SPL is lower than 80 dB, i.e. about 60 dB below the maximum SPL.

In terms of memory requirements, the memory usage for the full LEE run is of 6 Gb, while it is of 3 Gb for the LEE/LPE coupling run. Therefore, the coupled computation requires 50 % less memory than the full LEE simulation, which corresponds to the ratio of elements in the LEE region with respect to the whole domain. In terms of computational time, the total time required to factorise and solve the matrix system is 28.7 s for the full LEE solution and 16.9 s for the LEE/LPE coupling solution, which means a computational time reduction of 41.1% in the latter case.

## 5. Conclusions

This paper demonstrates the applicability of a novel coupling method dedicated to aeroengine exhaust noise predictions. The method is based on the combination of the Linearised Euler Equations and the Linearised Potential Equation, in order to optimise the computational cost. The LEE are used in the regions of strong mean-flow gradients, whereas the LPE applies in the regions where the mean flow is irrotational. The coupling strategy, presented for axisymmetric flow configurations, has been successfully applied to predict the noise radiated from an aeroengine exhaust. It is found to allow for the transmission of the acoustic waves between the LEE and the LPE subdomains, without the generation of spurious reflections. The benefits of this approach with respect to a full LEE model are also shown, with a gain of about 50% both in terms of memory usage and computational time. Promising results are thus expected when applying this coupling strategy to predict the

sound radiated from aeroengine exhausts using three-dimensional models.

## Acknowledgement

This project has been funded by the European Commission through the FP7-PEOPLE-ITN-2011 FlowAirS project, grant agreement 289352, coordinated by Y. Aurégan from the Laboratoire d'Acoustique de l'Université du Mans (France).

## References

- [1] ICAO. Environmental report. Technical report, International Civil Aviation Organization, Montréal, Quebec, Canada, 2010.
- [2] E. Envia, A.G. Wilson, and D.L. Huff. Fan noise: a challenge to CAA. *International Journal of Computational Fluid Dynamics*, 18(6):471–480, 2004.
- [3] H. Bériot, G. Gabard, and E. Perrey-Debain. Analysis of high-order finite elements for convected wave propagation. *International Journal for Numerical Methods in Engineering*, 96(11):665–688, 2013.
- [4] W. Eversman. *Theoretical models for duct acoustic propagation and radiation. Aeroacoustics of flight vehicles*, volume 2: Noise control. Acoustical Society of America, 1995.
- [5] K. Hamiche. *A high-order finite element model for acoustic propagation*. PhD thesis, University of Southampton, 2016.
- [6] A. Angeloski, M. Discacciati, C. Legendre, G. Lielens, and A. Huerta. Challenges for time and frequency domain aeroacoustic solvers. In *WCCM XI*, 2014.
- [7] S.W. Rienstra. Impedance models in time domain including the extended Helmholtz resonator model. In *12th AIAA/CEAS Aeroacoustics Conference, paper AIAA-2006-2686*, 2006.
- [8] P. Solin, K. Segeth, and I. Dolezel. *Higher-order finite element methods*. CRC Press, 2003.
- [9] J. Donea and A. Huerta. *Finite element methods for flow problems*. John Wiley & Sons, 2003.
- [10] R. Codina. Comparison of some finite element methods for solving the diffusion-convection-reaction equation. *Computer Methods in Applied Mechanics and Engineering*, 156(1-4):185–210, 1998.
- [11] P.P. Rao and P.J. Morris. Use of finite element methods in frequency domain aeroacoustics. *AIAA Journal*, 44(7):1643–1652, 2006.
- [12] J.-P. Bérenger. A perfectly matched layer for the absorption of electromagnetic waves. *Journal of Computational Physics*, 114(2):185–200, 1994.
- [13] M.E. Goldstein. An exact form of Lilley's equation with a velocity quadrupole/temperature dipole source term. *Journal of Fluid Mechanics*, 443:231–236, 2001.
- [14] K. Hamiche, G. Gabard, and H. Bériot. A high-order finite element method for the Linearised Euler Equations. *Acta Acustica united with Acustica*, 102(5):813–823, 2016.
- [15] S.W. Rienstra and A. Hirschberg. An introduction to acoustics. *Eindhoven University of Technology*, 2013.

- [16] K. Hamiche, G. Gabard, and H. Bériot. A higher-order finite element method for the Linearised Euler Equations. In *Proceedings of the International Conference on Noise and vibration Engineering ISMA 2014, Leuven, Belgium*, 2014.
- [17] The MathWorks Inc. *MATLAB R2013a*. Natick, MA, USA, 2014.
- [18] R.M. Munt. The interaction of sound with a subsonic jet issuing from a semi-infinite cylindrical pipe. *Journal of Fluid Mechanics*, 83:609–640, 1977.
- [19] G. Gabard and R.J. Astley. Theoretical model for sound radiation from annular jet pipe: far- and near-field solutions. *Journal of Fluid Mechanics*, 549:315–341, 2006.